Journal of Alzheimer's Disease xx (20xx) x–xx
DOI 10.3233/JAD-170563
IOS Press

Validation by Magnetic Resonance Imaging of the Diagnostic Potential of a Heptapeptide-Functionalized Imaging Probe Targeted to Amyloid-β and Able to Cross the Blood-Brain Barrier

Séverine André[a], Emilie Ansciaux[a,1], Elamine Saidi[a], Lionel Larbanoix[b], Dimitri Stanicki[a], Denis Nonclercq[c], Luce Vander Elst[a], Sophie Laurent[a,b], Robert N. Muller[a,b] and Carmen Burtea[a,*]
[a]*Department of General, Organic and Biomedical Chemistry, NMR and Molecular Imaging Laboratory, University of Mons, Mons, Belgium*
[b]*Center for Microscopy and Molecular Imaging, Gosselies, Belgium*
[c]*Laboratory of Histology, University of Mons, Mons, Belgium*

Accepted 21 August 2017

Abstract. The diagnosis of Alzheimer's disease (AD) is a critical step in the management of patients. We have developed a non-invasive diagnosis tool based on magnetic resonance molecular imaging (MRMI) of amyloid-β peptide using ultra-small particles of iron oxide (USPIO) functionalized with a disulfide constrained cyclic heptapeptide (PHO) identified by phage display (USPIO-PHO). After previously demonstrating the optimal pharmacologic properties of USPIO-PHO and its capacity to cross the blood-brain barrier (BBB), the ability of USPIO-PHO to target amyloid plaques (AP) by MRMI has been validated in the present work on AD transgenic mice. The immunohistochemistry and immunofluorescent detection of USPIO-PHO on brain sections collected after *in vivo* MRMI studies enabled its colocalization with AP, confirming the BBB passage and specific targeting. The AP targeting by USPIO-PHO has been moreover corroborated by the good correlation between the number of AP detected with anti-amyloid beta antibody and Perls'-DAB staining. Finally, the crossing mechanism of USPIO-PHO through the BBB was elucidated, revealing the involvement of non-degradation pathway of caveolae, while the control contrast agent USPIO-PEG was not endocytosed by the human brain endothelial cells.

Keywords: Alzheimer's disease, amyloid-β peptide, blood-brain barrier, contrast agents, functionalized iron oxide nanoparticles, magnetic resonance imaging

INTRODUCTION

Among all dementias, Alzheimer's disease (AD) is the biggest killer worldwide and constitutes a global health problem. Every year, 9.9 million people are diagnosed with AD in both developed and developing nations due to the population aging [1, 2]. Current concerns are imperative from both scientific and economic points of view, and require significant advances of both therapeutic and diagnosis tools. Currently, the main challenge is to improve the AD diagnosis that is late and definitive only after postmortem examination. The initial diagnosis is presumptive and based on clinical and neuropsychological

[1]Present address: Bone Therapeutics, Gosselies, Belgium.

*Correspondence to: Professor Carmen Burtea, Department of General, Organic and Biomedical Chemistry, NMR and Molecular Imaging Laboratory, University of Mons, Avenue Maistriau 19, Mendeleïev Building, B-7000 Mons, Belgium. Tel./Fax: +32 65373524; E-mail: Carmen.burtea@umons.ac.be.

ISSN 1387-2877/17/$35.00

evaluations, but there is no routine screening, and diagnosis is often performed on the basis of symptoms observed by the patient's relatives. At this late time point, the disease is too advanced because of high neuronal loss, decreasing the outcome of symptomatic treatments available today [3].

The amyloid hypothesis sustains that excessive production or impaired catabolism of amyloidogenic fragments (amyloid-β peptides, i.e., $A\beta_{40}$ and $A\beta_{42}$) of the amyloid-β protein precursor (AβPP) initiates the pathogenic cascades, causing neuronal dysfunction and neurodegeneration [1, 4–6]. Being more hydrophobic and fibrillogenic, $A\beta_{42}$ is the major constituent of amyloid plaques (AP) that are one of the main hallmarks of AD [7–9]. During the pathogenesis process, $A\beta_{42}$ accumulates and aggregates in numerous deposits within the brain. The formation of these plaques is one of the first molecular events in AD and precedes by at least 10 years the apparition of the first clinical symptoms. It is why AP monitoring is the main predictive and specific biomarker of AD. Therefore, many efforts were dedicated during the last decade to develop specific probes able to detect $A\beta_{42}$ deposits by trying to improve the specificity and the precocity of AD diagnosis.

Due to its high sensitivity, nuclear imaging provides tools for early detection of pathological biomarkers and for ruling out other pathologies. Several positron emission tomography (PET) tracers (PIB compound, SB13 labelled with 11-carbon, BF-227 labelled with 11-carbon, FDDNP labelled with 18-fluor) were developed in the last decade to detect $A\beta_{42}$ deposits [10].

Near infrared fluorescence (NIRF) imaging is a low cost, fast, and safe alternative to nuclear imaging methods. In this light window, the sensitivity is optimal because the tissue autofluorescence is limited and the light penetration is maximized. Some Aβ-targeted NIRF probes were developed and evaluated in AD mouse models [11]. Unfortunately, NIRF approach has limited use in human diagnosis because of a detection depth limited to a few centimeters.

Due to its high anatomical resolution, large penetration depth, and its typical non-invasiveness which enables iterative patient monitoring, magnetic resonance imaging (MRI) seems to be an optimal alternative to nuclear and NIFR imaging technologies. MRI contrast agents (CA) can be engineered to perform high resolution molecular imaging and, among them, ultra-small particles of iron oxide (USPIO) offer the highest sensitivity and low toxicity. To bind AP, MRI CA were linked to $A\beta_{42}$ [12] or a fragment of Aβ [13] using the intrinsic property of Aβ to self-aggregate. Other CA were vectorized with an anti-amyloid antibody [14]. However, these large molecules are highly immunogenic and have short half-lives once injected. Furthermore, they do not pass through the blood-brain barrier (BBB) and some invasive drugs, such as mannitol, have to be co-injected. Indeed, crossing the BBB is one of the main challenges when targeting structures in the brain. The exchange between blood compartment and brain parenchyma is very restrictive because of the particular structure of the cerebral capillary endothelium, i.e., the absence of fenestration, the presence of efflux active pumps, the low level of pinocytosis vesicles and the high level of specific transport. Consequently, only very small hydrophobic compounds can pass passively through the BBB, whereas larger molecules cross this biological barrier through transcytosis mechanisms involving specific-receptors. Astrocytic endfeet processes and mesenchymal-like cells pericytes play also a key role in the control of molecular transit across the BBB.

In aiming to solve the limitations of the previously proposed MRI CA and develop a complementary tool for PET tracers already approved for clinical implementation, we have searched for original low-molecular weight peptide vectors, known for their optimal pharmacologic properties, such as the reduced immunogenicity, toxicity, and *in vivo* retention. By coupling them to USPIO, the new CA could attain a targeting affinity and imaging sensitivity comparable to those of nuclear probes. To achieve this goal, the phage display technology has been previously employed by our group to screen small peptide (i.e., 6-7 amino acids) libraries for their affinity to $A\beta_{42}$ [15]. Three peptides (named PHO, PHI, and P1) were selected based on their promising $A\beta_{42}$ targeting skills, and they were coupled to USPIO with the goal to develop MRI CA for AD diagnosis. After a large panel of *in vitro* and *in vivo* evaluations, USPIO-PHO was selected because of its optimal pharmacologic properties, namely the lack of toxicity, both *in vitro* and *in vivo*; a high affinity against its target, the $A\beta_{42}$; pharmacokinetic parameters that allow its accumulation in the brain; and a capacity to cross the BBB without any crossing strategy [16]. If successful, the new MRI tracer could contribute to the non-invasive AD diagnosis via the detection of the brain's amyloid burden with high sensitivity (characteristic to USPIO CA) and anatomical resolution (characteristic to MRI technique). Moreover, this new imaging probe could additionally be

functionalized with PET tracers for a multimodal amyloid visualization with hybrid PET/MRI scanners recently introduced for clinical applications, offering novel perspectives for more accurate AD diagnosis.

In the present work, USPIO-PHO was evaluated on AD mouse models (TG2576, APP/PS1 dE9, and triple transgenic APP/PS1/Tau) in order to validate its diagnostic ability by MRI. The correlation between immunohistochemistry detection of AP on brain sections and USPIO-PHO binding to the same AD biomarker enabled us to quantify the potential of USPIO-PHO to discriminate the level of $A\beta_{42}$ deposition and thus the disease severity. The colocalization of USPIO-PHO with $A\beta_{42}$ aggregates, including AP, was assessed by immunofluorescence and compared to a non-functionalized CA to validate its specificity. USPIO derivatives were all rendered stealth by surface coating with poly(ethylene glycol) (PEG), which improves the specific biomarker targeting by preventing USPIO opsonization and the clearance by the reticuloendothelial system.

MATERIAL AND METHODS

Synthesis of USPIO derivatives

USPIO derivatives were synthesized as previously described [16–20]. Briefly, the 8-amino-3,6-dioxaoctanoyl (two PEG units) derivative of peptide PHO (PolyPeptide Strasbourg, France) was covalently conjugated via its N-terminus to the carboxyl groups exposed at the surface of USPIO to obtain USPIO-PHO. A PEG coating [O-(2-aminoethyl)-O-methyl-polyethyleneglycol, Mw $\sim$ 750 g/mol, Sigma-Aldrich, Bornem, Belgium] was then added onto the free reactive groups of USPIO. USPIO coupled with PEG only (USPIO-PEG) was used as a negative control. For *in vitro* fluorescence assays, rhodamine was added to our USPIO constructs (USPIO-PHO-rho and USPIO-PEG-rho) as described by Stanicki et al. [21]. For this purpose, a grafting step of rhodamine derivative is added before the PEG coating.

Molecular imaging by MRI of $A\beta_{42}$ in the brain of animal models of AD

Mouse models of AD and experimental groups

All *in vivo* experiments fulfil the requirements of the UMONS Animal Care and Use Committee and adhere to the national and international laws and provisions regarding the protection of animals. Three transgenic mouse models (only males) were used in these studies: (1) TG2576 mice [B6;SJL-Tg2576Kha (APPSWE)]; (2) APP/PS1 dE9 mice [B6.Cg-Tg(APPswe, PSEN1dE9)85Dbo/J], both strains kindly provided by Guerbet company (Aulnay-sous-Bois, France); and (3) APP/PS1/Tau [B6;129-$Psen1^{tm1Mpm}$ Tg(APPswe, tauP301L)1Lfa/Mmjax], purchased from The Jackson Laboratories (Maine, USA). TG2576 mice overexpress the isoform 695 of APP bearing the Swedish mutation (APPK670/671L); they present numerous AP by 11–13 months of age and progressive cognitive impairment by 9-10 months of age [22]. APP/PS1 dE9 mice overexpress a chimeric mouse/human APP695 bearing mutations linked to familial AD (KM593/594NL) and the human presenilin-1 carrying the exon-9 deleted variant; this strain presents an amyloid burden and cognitive impairment by 6-7 months of age [23]. APP/PS1/Tau mice are homozygous for APPSwe, presenilin-1 PS1M146V and protein tau P301L transgenes, and are supposed to exhibit AP (with intracellular $A\beta_{42}$ deposition by 3-4 months; extracellular deposits appear at 6 months), tangle pathology (between 12–15 months), and a cognitive decline similar to those observed in AD [24]. However, the supplier communicated several months after their acquisition that male mice may not exhibit these phenotypic traits, as confirmed by our studies (please see the results below).

Our experiments were performed on 24-month-old TG2576 and APP/PS1 dE9 mice, whereas APP/PS1/Tau mice were employed at 12 months of age. Considering that amyloid burden (the target of USPIO-PHO) is maximal in 24-month-old TG2576 and APP/PS1 dE9 mice, the *in vivo* data obtained on these strains were analyzed without any strain distinction. For simplicity, they were called AD mouse model (ADMM).

USPIO-PHO and USPIO-PEG were evaluated by MRI on eight ADMM mice, five of them being injected with USPIO-PHO, while USPIO-PEG was administered to three mice. In order to increase the brain access of USPIO-PHO, four more mice of the same strain were injected just after Cereport (a synthetic bradykinin analogue known to open transiently the BBB; BACHEM, Bubendorf, Switzerland). In the case of APP/PS1/Tau strain (called APTS), six mice were injected with USPIO-PHO, while USPIO-PEG was administered to three mice.

The CAs were injected in the tail vein at a dose of 200 μmol Fe/kg b.w, whereas Cereport was administered at a dose of 9 μg/kg b.w.

Molecular imaging of amyloid burden by MRI

For molecular imaging by MRI, mice were anesthetized with 2% isoflurane (Tem Sega, Lormont, France) at a rate of 70 ml/min. Mice respiration was monitored during all MRI experiments and the body temperature was maintained at 37°C with a warm water circulating system.

Subsequent to the acquisition of pre-contrast images, CAs were injected as described above, and the post-contrast images were acquired at the level of the head on a 300 MHz (7T) Bruker Pharmascan imaging system (Bruker, Ettlingen, Germany) equipped with a horizontal magnet and a circular polarized MRI transceiver coil (55 mm × 23 mm; frequency of 3 MHz; maximum RF of 5 ms), using the sequence RARE (Rapid Acquisition with Relaxation Enhancement) : TR/TE = 3000/30 ms, RARE factor = 4, NEX = 4, FOV = 2.5 cm, matrix = 512 × 512, slice thickness 1 mm, 20 axial slices, spatial resolution= 48 μm, TA = 25 min 36 s.

Analysis of contrast enhancement and of amyloid burden's molecular labelling

The contrast enhancement was calculated after measuring the signal intensity (SI) values, using the ImageJ software (National Institutes of Health, USA), on pre- (SI_{pre}) and post-contrast (SI_{psot}) MR images within regions of interest (ROI) drawn manually at the level of cortex, hippocampus, thalamus and the whole brain. The standard deviation (SD) of the noise was measured in a region outside of the animal body. These values were used to compute the percentage change of the Signal-to-Noise Ratio (SNR) on post-contrast as compared to pre-contrast images according to the following equation:

$$\Delta\mathrm{SNR}\% = \left[\frac{\left(\mathrm{SI_{post}}/\mathrm{NoiseSD}\right) - \left(\mathrm{SI_{pre}}/\mathrm{NoiseSD}\right)}{\mathrm{SI_{pre}}/\mathrm{NoiseSD}}\right] \times 100$$

Aiming to quantify the molecular labelling produced by USPIO-PHO on amyloid burden, the total number of black pixels was determined for cortex, hippocampus, thalamus, and the whole brain using the ImageJ software [17, 19]. The level of black pixels in post-contrast images has been thresholded to the pre-contrast level, and the results were automatically provided by ImageJ software after image segmentation (Supplementary Figure 1). The results were expressed as percentage of black pixels in post-contrast compared to pre-contrast images.

Detection of amyloid plaques and peptide by immunohistochemistry

About three weeks subsequent to the MRI studies, the mice were reinjected with USPIO derivatives as described above and euthanized 90 min later by a lethal dose of Nembutal (Sanofi, Brussels, Belgium). Considering that the total imaging time lasted for more than 2 h, this experimental strategy was justified by the selection of the optimal brain uptake of the CA observed during our present and previous MRI and biodistribution studies [16]. The blood was removed, tissues rinsed by a transcardial perfusion of 10 ml of phosphate buffered saline (PBS, per liter: 8 g NaCl, 0.2 g KCl, 2.31 g $Na_2HPO_4 \times 12\ H_2O$, 0.2 g KH_2PO_4, pH 7.4), and the brains were harvested in 4% paraformaldehyde. Subsequent to the alcohol and butanol baths, the brains were paraffin embedded and cut to obtain 5 μm slices.

The presence of AP in the brains of transgenic mice was verified on histological sections through the detection of Aβ by an anti-$A\beta_{17\text{-}24}$ antibody (clone 4G8, Eurogentec, Seraing, Belgium). For this purpose, brain slices were rehydrated and endogenous peroxydases were blocked 15 min with 0.15% H_2O_2 in PBS and rinsed two times for 5 min in PBS-0.1% Tween-20. Brain slices were blocked with PFBB (Pierce Protein-Free Blocking Buffer, Thermo Fisher Scientific, p/a Perbio Science BVBA, Aalst, Belgium) for 1 h before overnight incubation with mouse anti $A\beta_{17\text{-}24}$ antibody at a concentration of 2 μg/ml. After rinsing three times for 5 min in PBS-0.1% Tween-20, slices were incubated for 1 h at room temperature with peroxidase-conjugated anti-mouse antibody (Vector Labconsult, Brussels, Belgium) at a concentration of 4 μg/ml. AP were then detected by treating tissues for 20 min with 0.05% 3,3'-diaminobenzidine (DAB) tetrachlorhydrate (Sigma-Aldrich) supplemented with 0.02% H_2O_2 prepared in PBS, pH 7.4. After rinsing again three times in distilled water, the sections were counterstained with Mayer's Hemalun (VWR International, Leuven, Belgium) and Luxol Fast Blue and mounted in a permanent medium (Leica Microsystems, Groot Bijgaarden, Belgium). Images were obtained using a Leica DM2000 microscope equipped with a DFC 425C camera and a light source EL 6000 (Leica Microsystems).

Perls'-DAB staining of USPIO derivatives on histological brain samples

USPIO derivatives present inside the brain parenchyma of the injected mice (please see the above

section for details) were revealed by Perls'-DAB iron staining on consecutive histological slices. For this purpose, they were rehydrated and endogenous peroxidases were blocked for 15 min with 1% H_2O_2 in PBS. USPIO derivatives were then detected by staining for 30 min with Perls' working solution (mixing equal volumes of 5% potassium ferrocyanide and 5% HCl). After rinsing three times for 10 min in distilled water, tissues were treated for 10 min with 0.05% DAB in PBS, pH 7.4, followed by immersion for 10 min in 0.05% DAB supplemented with 0.033% H_2O_2 prepared in PBS, pH 7.4. After rinsing again in distilled water, the sections were counterstained with Hemalun and Luxol Fast Blue and mounted in a permanent medium.

Colocalization of AP and vectorized contrast agents by immunofluorescence

After rehydration, histological sections were blocked with 1% bovine serum albumin (BSA, Sigma-Aldrich) in PBS for 1 h. Brain slices were then incubated overnight with rat anti-PEG (8 μg/ml, Abcam, Cambridge, UK) and 4G8 mouse anti-$A\beta_{17\text{-}24}$ (5μg/ml, Eurogentec, Seraing, Belgium) antibodies diluted in PBS complemented with 0.5% BSA and 0.05% Tween-20. After rinsing three times with 0.1% Tween-20 in PBS, fluorescein-conjugated rabbit anti-rat mouse adsorbed and Texas Red-conjugated horse anti-mouse antibodies (Vector Labconsult) were incubated with brain slices for 1 h at a concentration of 20μg/ml in phosphate buffer (per liter: 0.304 g $Na_2HPO_4 \times 12\ H_2O$, 1.26 g $NaH_2PO_4 \times H_2O$, 8.76 g NaCl, pH 7.8). After rinsing again two times with PBS-0.1% Tween-20 and one time in PBS, histological tissues were mounted with Vectashield Mounting Medium with 4',6-diamidine-2'-phenylindole dihydrochloride (DAPI, Vector Labconsult). Fluorescence was observed using a Leica DM2000 microscope.

Colocalization of USPIO-PHO with caveolae and lysosomes in human brain microvascular endothelial cells

The human brain microvascular endothelial cells ACBRI376 (Cell Systems, Kirkland, WA, USA) were cultured in complete CSC medium (Cell Systems) supplemented with 1% Antibiotic-Antimycotic (Life Technologies, Gent, Belgium) and 2% CultureBoost (Cell Systems). For fluorescence assays, cells were seeded onto coverslips coated with 0.2 mg/ml collagen at a density of 1.5×10^5 cells/well. Cells were incubated with USPIO-PHO-rho or USPIO-PEG-rho (2 h, 37°C) at a concentration of 500μM in MCDB131 culture medium supplemented with 2% FBS, 1% L-glutamine, 0.14% heparin 5000 U/ml, and 1% antibiotic-antimycotic (all from Life Technologies). The negative control was incubated with USPIO-free culture medium. Cells were rinsed two times with PBS and fixed with 4% buffered formaldehyde (Sigma-Aldrich) for 5 min. Then, cells were rinsed again and blocked with PBS supplemented with 5% normal goat serum (Cell Signaling Technology, BIOKE, Leiden, Netherlands) and 0.3% Triton-X100 (Sigma-Aldrich). After rinsing steps, the detection of caveolae and lysosomes was performed using anti-caveolin 1 or anti-LAMP1 antibodies made in rabbit (both from Santa Cruz, Heidelberg, Germany) that were incubated overnight at a concentration of 4 μg/ml in PBS. Cells were rinsed again and incubated with 20 μg/ml of anti-rabbit IgG antibody made in goat coupled to fluorescein (Vector Labconsult) in phosphate buffer pH 7.8 supplemented with 0.5% BSA for 1 h. Finally, cells were rinsed and mounted with Vectashield Mounting Medium with DAPI.

Statistical analysis

All data are expressed as means ± standard deviation (SD). Differences between experimental groups were evaluated by one-way ANOVA using the software SigmaPlot 11.0. For groups where homoscedasticity was not validated, the statistic validation was confirmed by Holm-Sidak and Bonferroni tests. Results are considered statistically different when $p < 0.05$.

RESULTS AND DISCUSSION

In vivo MRI evaluation of the functionalized imaging probe USPIO-PHO

The ability of USPIO-PHO to cross the BBB and detect AP has been evaluated by MRI on ADMM transgenic mice, USPIO-PEG being used as a negative control. Figure 1A shows the global darkening of the brain on post-contrast images compared to the pre-contrast ones. The overall negative contrast produced by USPIO-PHO was persistent until the end of the imaging session (130-min post-injection), whereas that produced by USPIO-PEG was evident at 30-min post-contrast, but lower than in USPIO-PHO injected mice. In addition to the global darkening

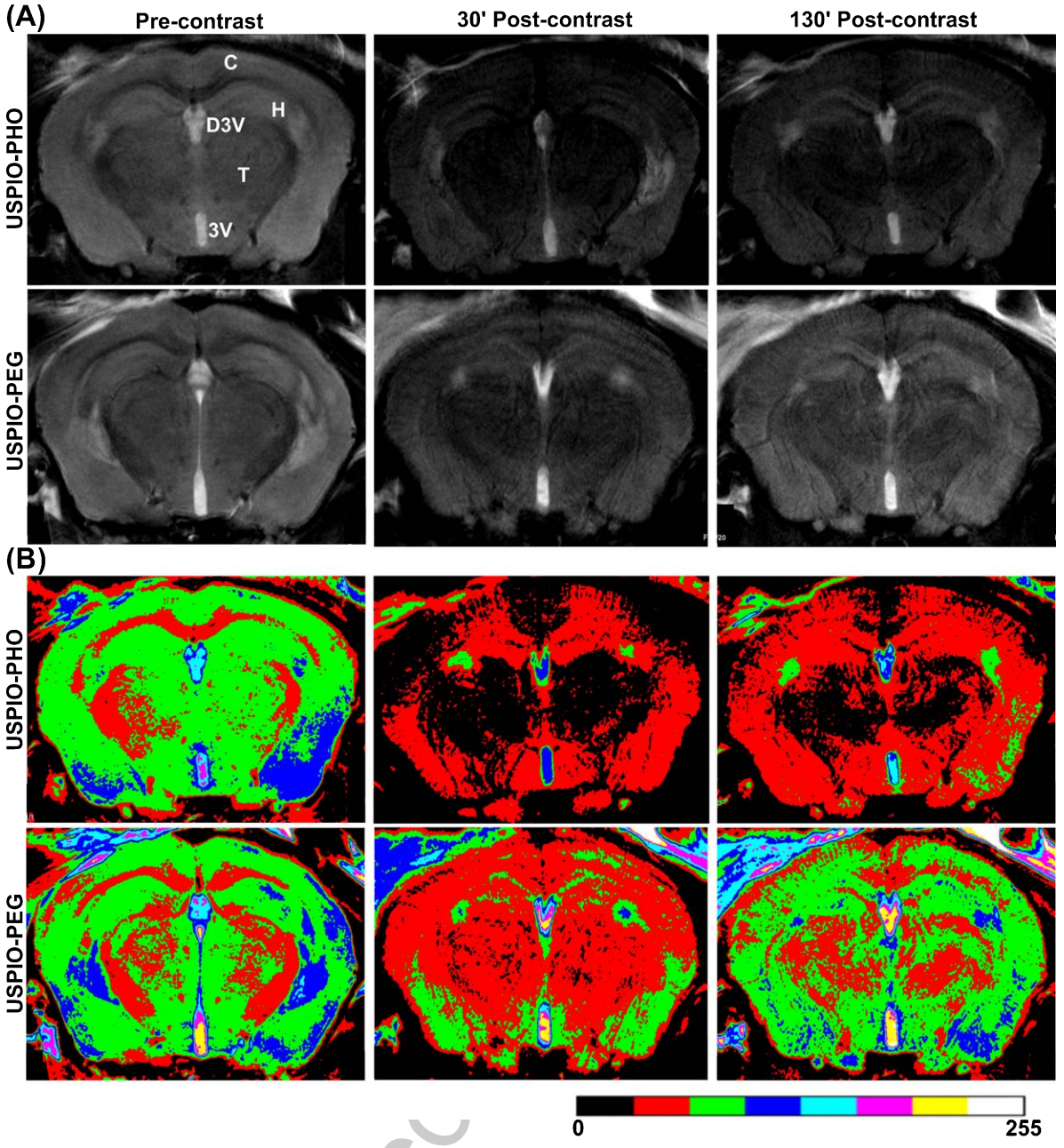

Fig. 1. MR images acquired with RARE protocol (spatial resolution = 48 μm), representative of the brain of ADMM transgenic mice, in pre-contrast and 30 or 130 min after their injection with USPIO-PHO or USPIO-PEG: (A) raw images; (B) color overlays of the raw images. The negative signal enhancement is observed on color overlays by the shift of colors from blue/green to black. C, cortex; H, hippocampus; T, thalamus; D3V, dorsal 3rd ventricle; 3V, 3rd ventricle.

of brain tissue in post-contrast images, the color overlays shown in Fig. 1B reveal the presence of dense dark spots in the cerebral cortex, hippocampus, and thalamus of the mice injected with USPIO-PHO, which correspond to its concentration at the targeted sites. Their density diminishes at 130-min post-contrast, but is still obvious and not reproduced by USPIO-PEG, which seems to be cleared from the brain at the same time post-injection.

The same *in vivo* MRI experiment has been reproduced on APTS mice which were supposed to exhibit Aβ and neurofibrillary tangle pathology similar to

those observed in AD patients by 6 months of age. The Supplementary Figure 2A shows MR images acquired in pre- and post-contrast, after the injection of USPIO-PHO or USPIO-PEG. The negative contrast produced by USPIO-PHO is much less important on this mouse model compared to ADMM mice and is similar to that observed previously on NMRI mice [16] (Fig. 2B), being explained by the lack of AP as confirmed by immunohistochemistry (please see the next section). This convinced us to use APTS mice as negative controls of AD pathology. Nevertheless, USPIO-PHO shows a slightly higher negative contrast as compared to USPIO-PEG due to the natural BBB crossing.

The negative contrast enhancement (ΔSNR%) measured on RARE images of the brain in ADMM transgenic mice (Fig. 2A) confirms that USPIO-PHO produced a much stronger effect than USPIO-PEG ($p < 0.05$) on ΔSNR% of all the analyzed brain regions (cortex, hippocampus, thalamus, the whole brain) and acquisition times. However, the maximum effect produced by USPIO-PHO on ΔSNR% of brains in APTS mice (Fig. 2B) is less important (i.e., –32% in the cortex at 100-min post-contrast) as compared to ADMM mice (–55% in the cortex at 130-min post-contrast), corroborating thus the empirical observation of MR images.

As previously observed by our group [16], USPIO-PHO attains a pick of brain penetration 90-min post-injection and is cleared from it 24 h later. The brain clearance 24-h post-injection has been confirmed within the present work on transgenic mouse models of AD (data not shown) and is in agreement with the elimination half-life ($T_{e1/2}$) of USPIO-PHO, which is about 3 h (versus about 5 h for USPIO-PEG) [16]. Although USPIO-PEG has a much longer elimination half-life (and thus a delayed blood clearance), it is not able to produce a comparable negative contrast on the brains of ADMM mice at imaging times later than 2 h.

All these experimental data strengthen the assumption that the contrast observed with USPIO-PHO in ADMM mice is not a consequence of the delayed blood clearance, but the result of $A\beta_{42}$ binding. The vectorization of USPIO with peptides speeds the rate of biomarker targeting, which allows diagnosis imaging in a clinical time window (i.e., 1-2 h post-injection), enhances the blood clearance and urine excretion, and restrains USPIO's uptake by the reticuloendothelial system (this last property in conjunction with PEG grafting) [16, 17, 19]. All these properties optimize the specific targeting and imaging of molecular biomarkers with functionalized nanoparticles, contributing in this way to a better non-invasive diagnosis.

Aiming to quantify the ability of USPIO-PHO to detect its molecular target by MRI, the total number of black pixels in post-contrast images has been determined by ImageJ and expressed in percentage compared to pre-contrast after thresholding them to the pre-contrast level of grey (Fig. 3). The percentage of black pixels is much larger in mice injected with USPIO-PHO as compared to USPIO-PEG at both image acquisition times (i.e., 30 and 130 min) and is statistically significant when measured on the entire brain and hippocampus; in cortex and thalamus, the difference is statistically significant ($p < 0.05$) at 30-min post-injection. These results suggest that the negative contrast produced by USPIO-PHO on the AD brain in experimental conditions reflects the specific imaging of its brain target, i.e., the Aβ aggregates.

The strong and extended negative contrast observed within the thalamus may be related to the supply of a larger quantity of USPIO-PHO in this brain area in conjunction to its retention by $A\beta_{42}$, as shown by immunohistochemistry studies (please see below). The blood is supplied to the thalamus via the posterior cerebral arteries, which derive from the basilar artery formed from the fusion of the two vertebral arteries. Branches of the posterior cerebral arteries deliver the blood to the posterior areas of the cortex too, after supplying the thalamus due to the anatomical topology. The blood supply to the middle and frontal parts of the cortex derives from branches of the internal carotid artery, which additionally receives blood from the posterior cerebral arteries via the posterior communicant arteries. The thalamus is therefore supplied with blood before the cortex due to its anatomical topology, which explains this spatio-temporal biodistribution of nanoparticles. Moreover, the thalamus delivery is facilitated by the larger diameter of the blood vessels at this level as compared to those in the cortex.

To increase the access to the brain of USPIO-PHO, a second study by MRI was performed using Cereport, which was injected to ADMM mice just before the administration of CA. Also called RMP-7 or labradimil, this molecule is a synthetic agonist of bradykinin B2 receptor that modulates tight junctions between endothelial cells and increases transiently the BBB permeability [25, 26]. Although quite variable, Cereport generally enhanced the negative contrast produced by USPIO-PHO in the brain

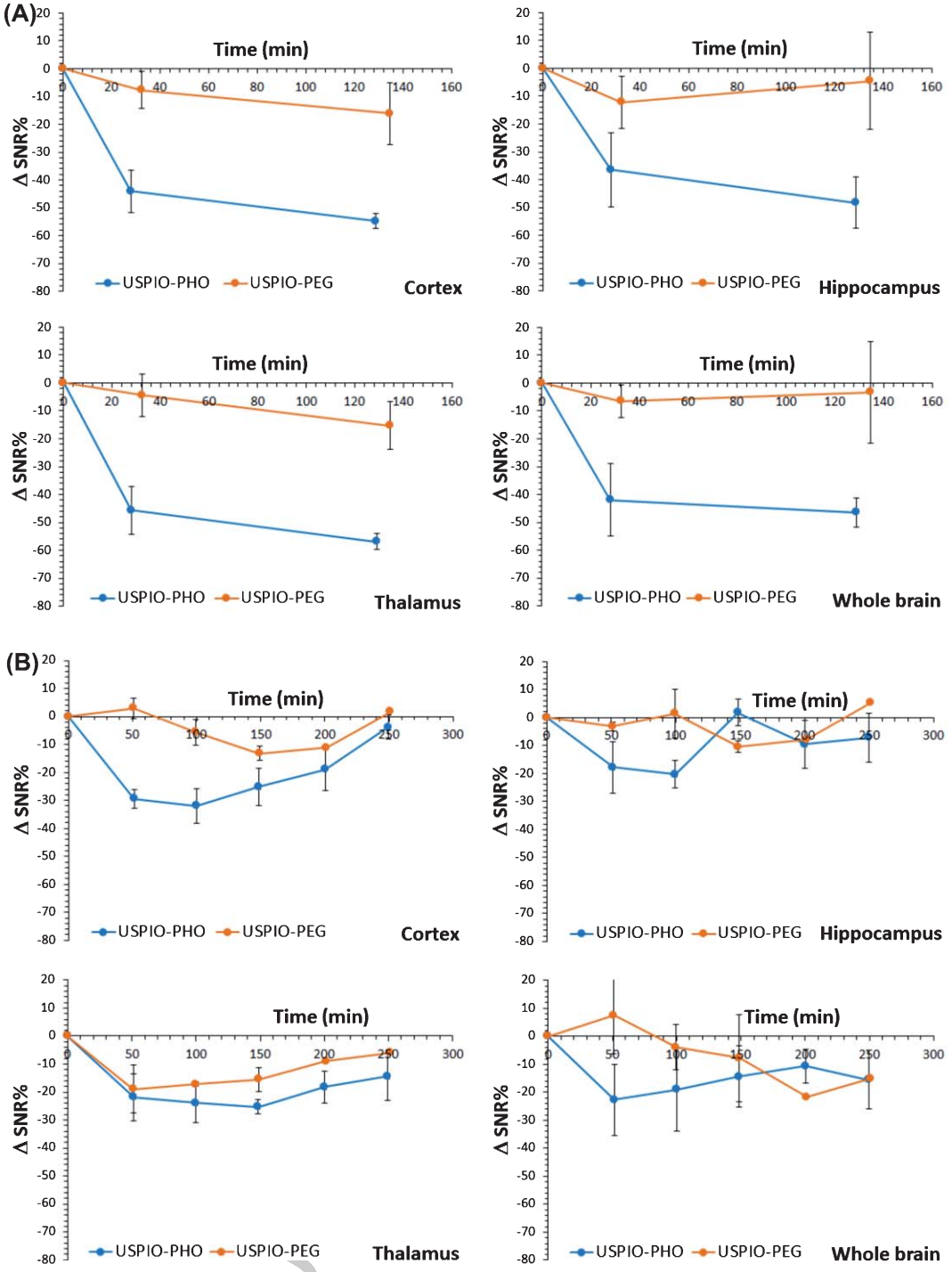

Fig. 2. Contrast enhancement (ΔSNR%) measured on different regions of the brain (cortex, hippocampus, thalamus, the whole brain) in MR images of ADMM (A) or APTS (B) transgenic mice injected with USPIO-PHO or USPIO-PEG.

of ADMM mice, at least during the first 105-min post-injection (Fig. 4), attesting thus its permissive effect at the level of BBB. The increase of ΔSNR% to lesser negative values 145-min post-injection suggests that Cereport facilitates the clearance of USPIO-PHO from the brain at times longer than

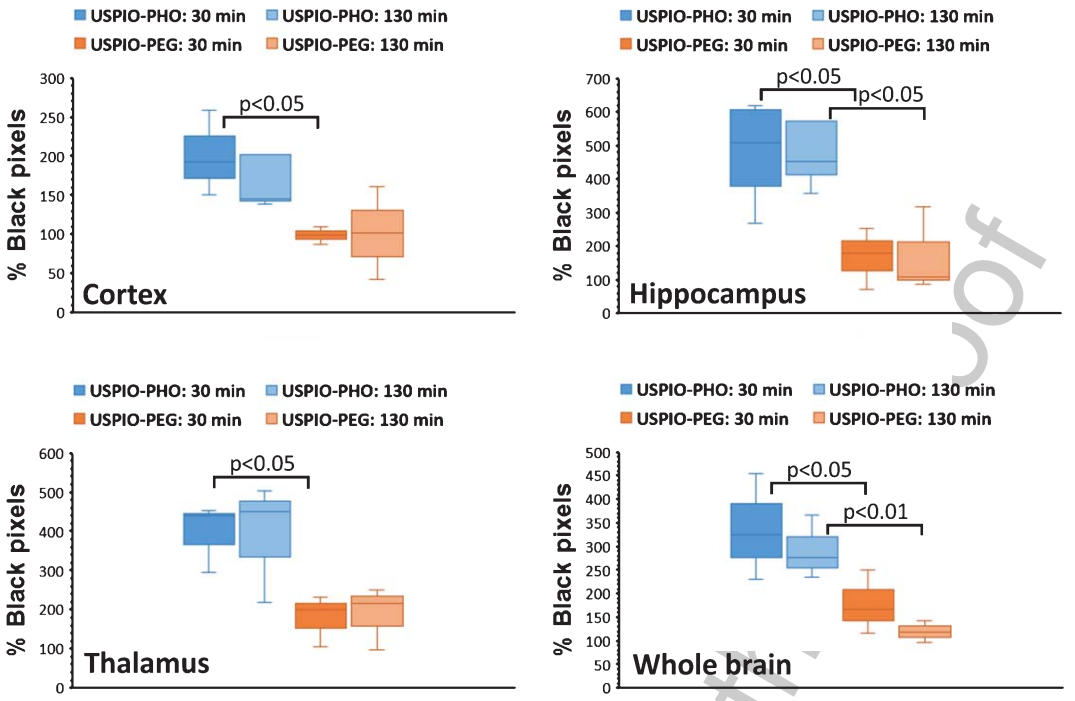

Fig. 3. The percentage of black pixels in post-contrast MR images of the brain of ADMM transgenic mice at different post-injection times of USPIO-PHO or USPIO-PEG (please see methods for the analysis of black pixels by ImageJ).

2 h after administration (Supplementary Figure 3). This result agrees with the published literature, which reported decreased levels of platinum in rat glioma 2 h after Cereport infusion [25]. On the other hand, the strong global negative contrast produced by USPIO-PHO at shorter acquisition times rendered difficult the interpretation of AP molecular imaging by MRI. Nevertheless, Cereport may be useful to increase the access to the brain of functionalized imaging probes and to perform specific molecular diagnosis at shorter times after injection if lower doses of CA are employed.

Validation of the transgenic mouse model by immunohistochemistry

The presence of AP and Aβ aggregates in the brain of ADMM and APTS mice has been evaluated by immunohistochemistry using an anti-$A\beta_{17-24}$ antibody. As shown in Fig. 5, ADMM mice are characterized by a high density of AP and Aβ aggregates mainly within the cortex and hippocampus, while the brain of APTS mice is void of this AD biomarker or of any evident pathological alteration, being similar to that of control NMRI mice. In addition to AP, Aβ seems to be diffusely concentrated in the cell bodies or aggregated between several cells or over the cell bodies. At a closer look, this Aβ distribution is also present in the thalamus (Supplementary Figure 4), where it is diffusely dispersed and forms less compact aggregates; it is moreover present in the endothelial cells of blood vessels, where USPIO-PHO was also observed (please see the next section). The vascular deposition of Aβ is a recognized feature of AD pathology [27]. Altogether, these results corroborate the MRI observations and contribute to the validation of specific AP/Aβ targeting by USPIO-PHO.

Perls'-DAB staining of USPIO derivatives on histological brain samples

The targeting of AP and Aβ aggregates by USPIO-PHO in the brain of ADMM mice pre-injected with this CA has been evaluated by Perls'/DAB staining of brain sections (Fig. 6). The dark staining of iron contained in USPIO-PHO corresponds to AP, but also to the brain parenchyma, reproducing the cell distribution of Aβ aggregates observed above with anti-$A\beta_{17-24}$ antibody (Fig. 5). USPIO-PHO was also observed in the endothelial cells of brain capillaries and surrounding parenchyma, and even in some cell bodies of neurons (Fig. 6, Supplementary Figure 5).

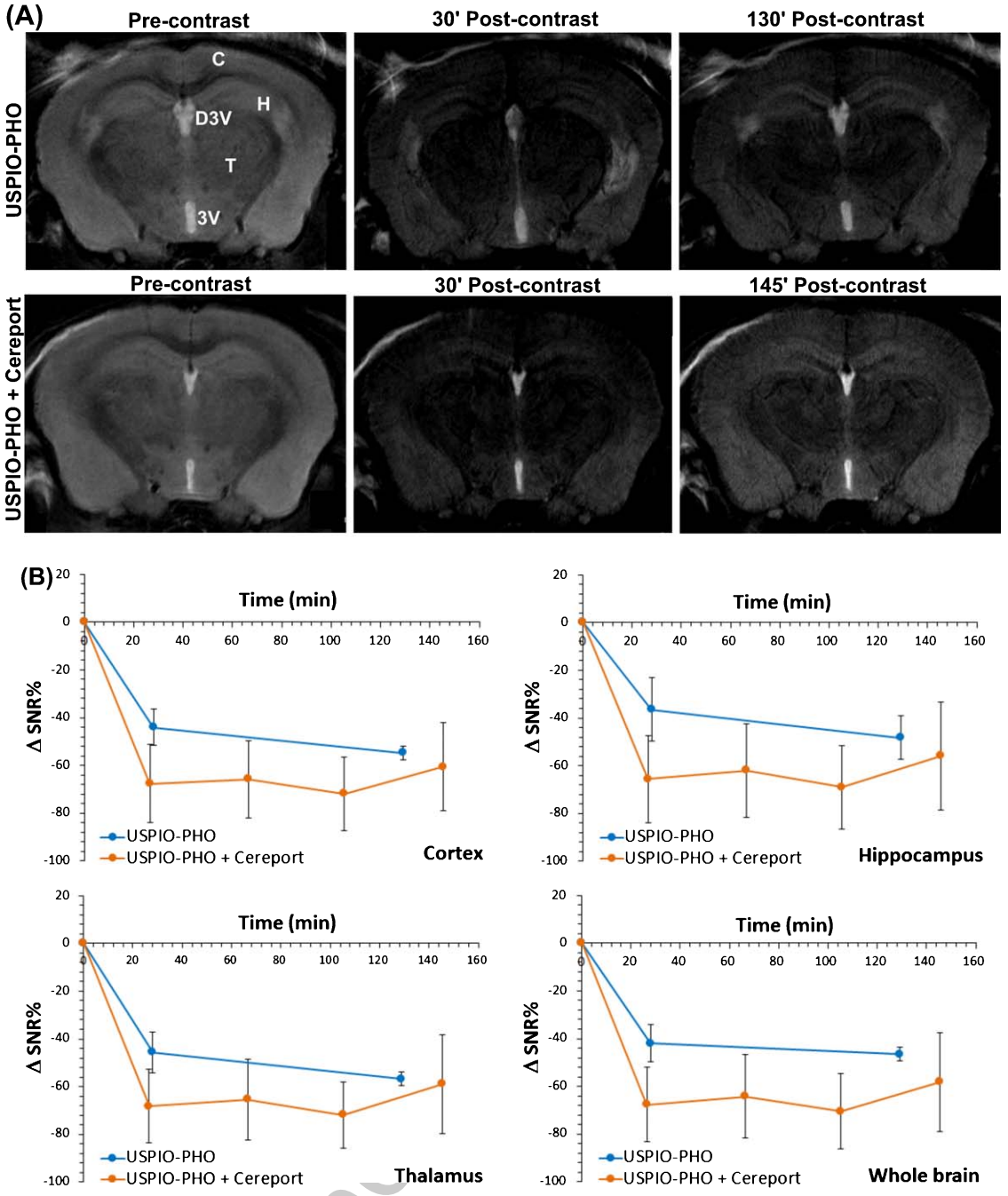

Fig. 4. MR images of the brain of ADMM transgenic mice injected with Cereport to enhance the BBB permeability for USPIO-PHO (A) and contrast enhancement (ΔSNR%) measured on different regions of the brain (cortex, hippocampus, thalamus, whole brain) in MR images acquired in these conditions (B). The MR images and ΔSNR% are compared with those obtained in the absence of Cereport.

USPIO-PEG was found rarely bound to AP, almost at their border, where the level of Perls'-DAB staining is significantly lower when compared to USPIO-PHO. To note that AP stained by USPIO-PEG shown in Fig. 6 are among the rare examples that could be identified; no staining of Aβ aggregates could be observed in the presence of this CA. As opposed to USPIO-PHO, USPIO-PEG was not identified in the endothelial cells of brain capillaries, but it could be detected within the lumen of these blood vessels

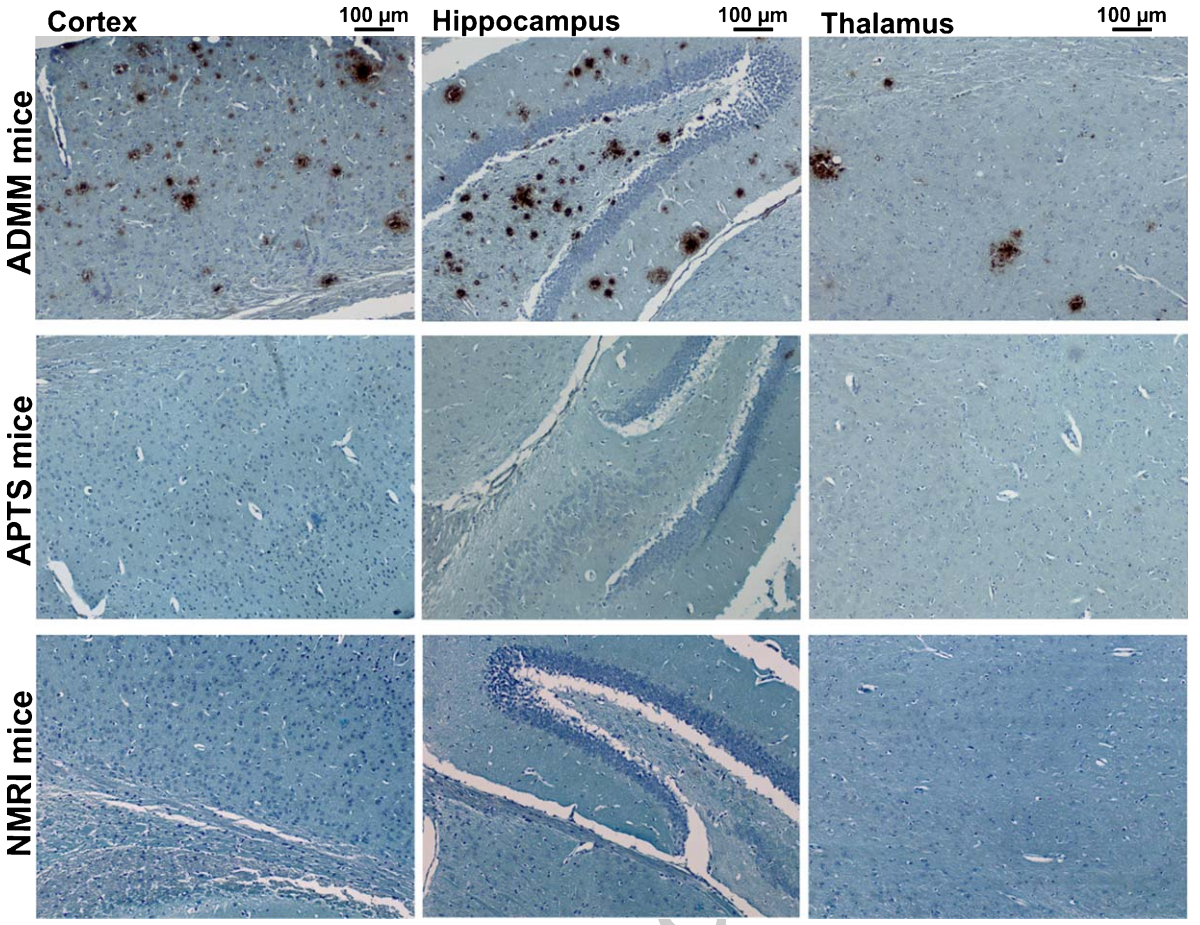

Fig. 5. Detection of AP and Aβ aggregates by immunohistochemistry in the cortex, hippocampus, and thalamus on brain slices of ADMM mice is compared to APTS and NMRI mice, used as control. AP and Aβ aggregates are stained in brown by DAB.

(Supplementary Figure 4). AP in USPIO-free control mice did not show any background staining of iron, supporting the assumption that USPIO-PHO is able to cross the BBB and target AP and Aβ aggregates. The presence of USPIO-PHO within endothelial cells of brain capillaries substantiates these observations.

Manual counting of AP stained by Perls'-DAB or by the 4G8 anti-$A\beta_{17\text{-}24}$ antibody (Fig. 7A) in the brain of ADMM mice reveals that USPIO-PHO is bound to about 50% of AP at 90-min post-injection; higher levels of detection with USPIO-PHO were obtained in thalamus, but this may be related to the smaller number of AP associated to this brain region, thus increasing the count precision. The same analysis performed on brain slices of mice injected with Cereport before USPIO-PHO confirms that Cereport amplified the brain clearance of nanoparticles as observed by MRI, since their binding to AP diminished to half or more than half when compared to USPIO-PHO alone. High correlation coefficients were found between the number of AP detected with anti-$A\beta_{17\text{-}24}$ 4G8 antibody or by Perls'-DAB staining (Fig. 7B), the highest corresponding to the cortex ($r^2 = 0.887$) and to the entire brain slice ($r^2 = 0.905$). Considering that Perls'-DAB staining detected USPIO-PHO nanoparticles bound to AP, one can assume that MRI investigations revealed the presence of this molecular hallmark of AD.

Colocalization between AP and vectorized contrast agents by fluorescence

The specific targeting of AP and Aβ aggregates in the brain of ADMM mice by USPIO-PHO was evaluated by immunofluorescence (Fig. 8). Aβ was colocalized with CA by co-incubation with anti-$A\beta_{17\text{-}24}$ and anti-PEG antibodies respectively on brain slices of the mice pre-injected with either

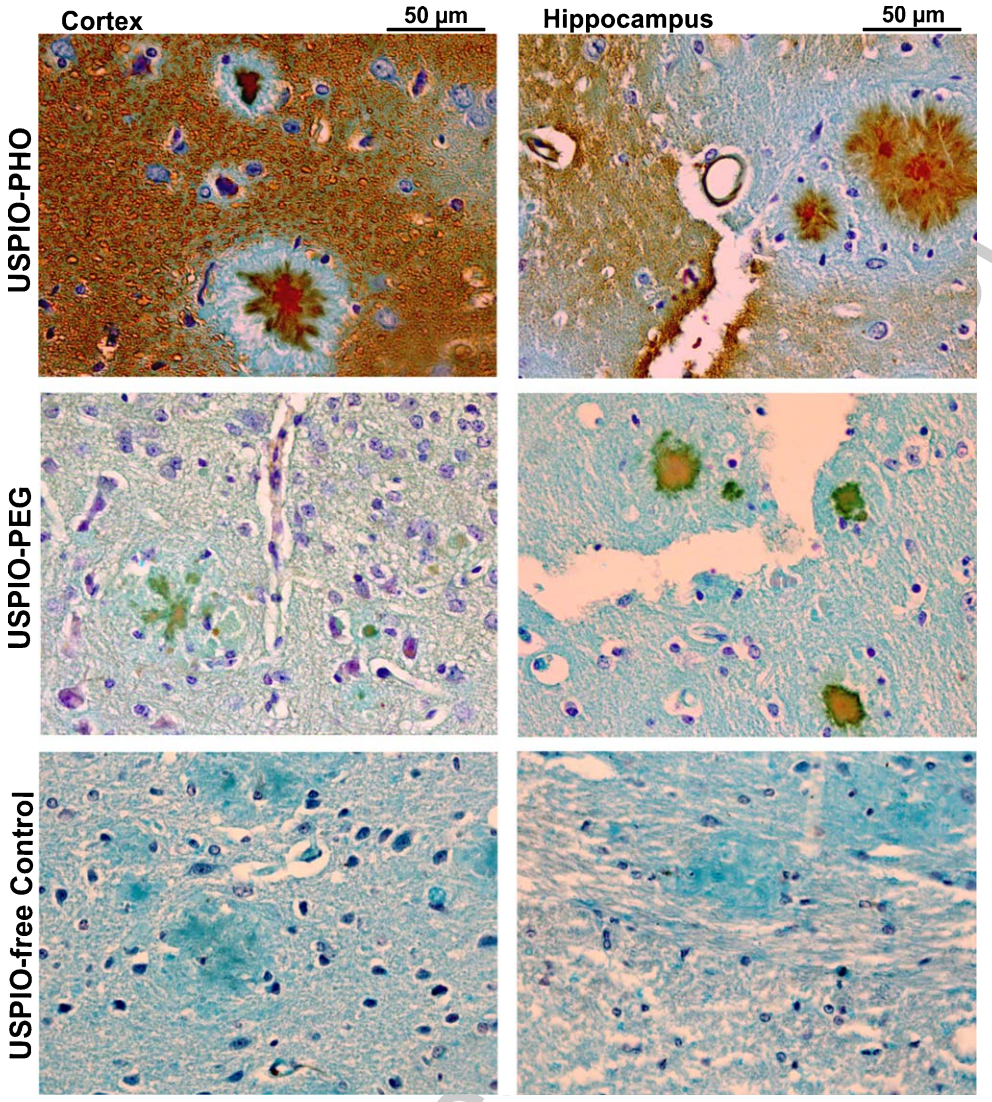

Fig. 6. Binding of USPIO-PHO to AP and Aβ aggregates in the brain (cortex and hippocampus) of ADMM mice was detected by Perls'-DAB staining and compared to USPIO-PEG and USPIO-free control mice. The iron contained in USPIO derivatives is stained in brown by Perls'-DAB protocol.

USPIO-PHO or USPIO-PEG. The results confirm that USPIO-PHO is located at the level of AP and Aβ aggregates, while USPIO-PEG could not be detected by this method probably because of the low concentration of PEG moieties, which are detected with anti-PEG antibody. Many of the cell nuclei located in the AP areas are pyknotic and fused to one another, demonstrating the cell death. Some cells seem to contain Aβ deposits in their cell bodies, which is consistent with the observation that Aβ is either generated intracellularly [28–30] or extracellularly, followed by its internalization by endocytosis [28, 30]. Upon intracellular aggregation of Aβ, this is released into the extracellular space subsequent to the cell lysis after death. The inclusion of cell nuclei in the amyloid deposits can also be observed in Fig. 5, although their identification is more challenging because the dark blue staining of nuclei is covered by the brown staining of Aβ.

In vitro evaluation of the transcytosis mechanism of USPIO-PHO through the BBB

In order to identify the cell compartment responsible of USPIO-PHO transcytosis over the endothelial cells of BBB, USPIO-PHO coupled to rhodamine

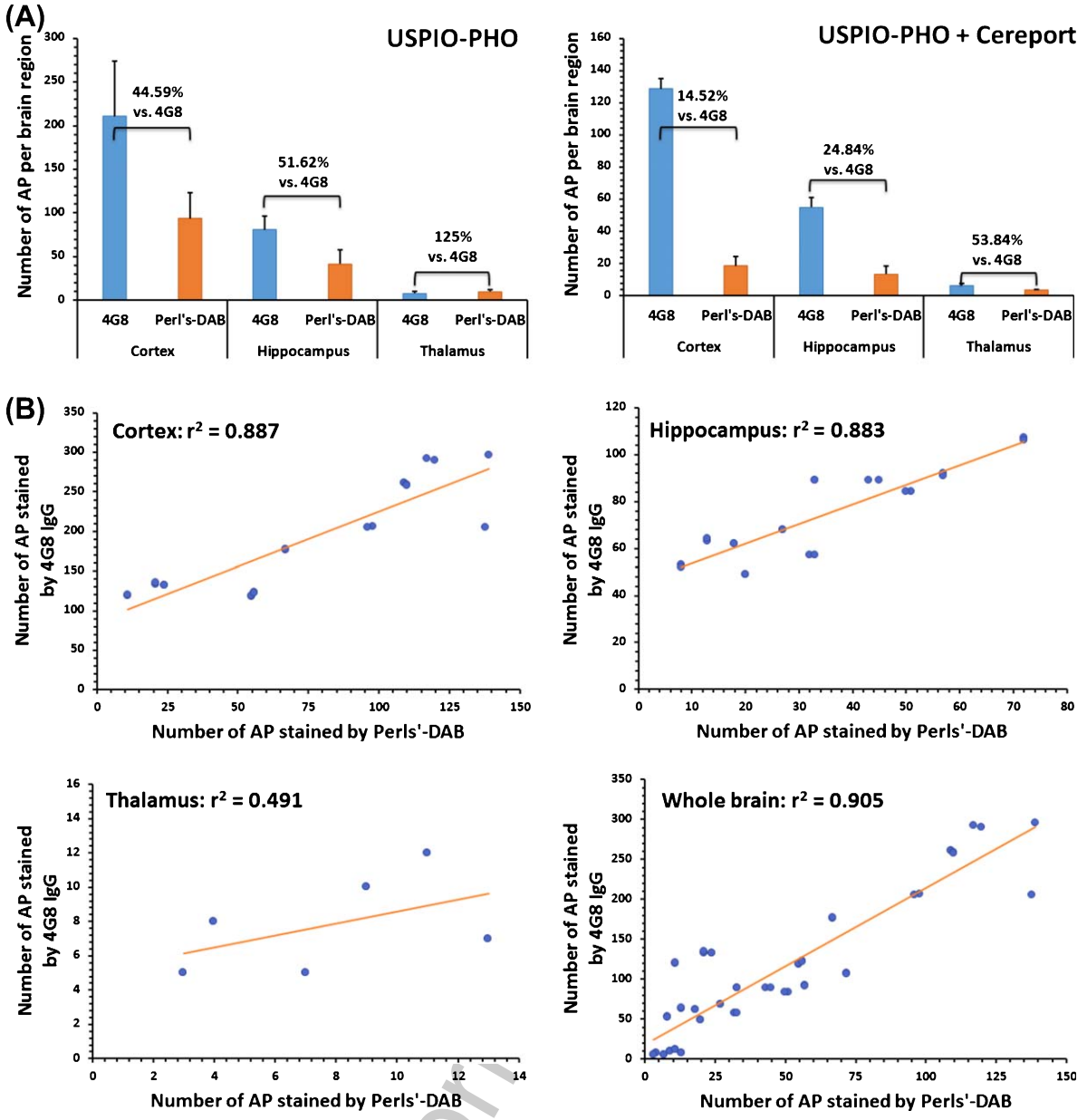

Fig. 7. Histograms showing the number of AP counted by microscopy in the brain (cortex, hippocampus, and thalamus) of ADMM mice injected with either USPIO-PHO (left) or USPIO-PHO and Cereport (right) after their detection with anti-A$\beta_{17\text{-}24}$ 4G8 antibody or by Perls'-DAB (A); the results are expressed as means of AP per mouse brain region ± SD; the percentage is calculated for Perls'-DAB versus anti-A$\beta_{17\text{-}24}$ 4G8 antibody stained AP. The correlation coefficients between the number of AP detected with anti-A$\beta_{17\text{-}24}$ 4G8 antibody or by Perls'-DAB staining are shown in (B).

(USPIO-PHO-rho) was colocalized with caveolae and lysosomes in ACBRI376 human brain microvascular cells (Fig. 9); USPIO-PEG-rho was used as a control CA. The results reveal that most parts of USPIO-PHO-rho are endocytosed via caveolae (Fig. 9A), and to a much lesser extent by lysosomes (Fig. 9B). In the case of caveolae, caveolin-1 seems to concentrate around the packs of USPIO-PHO-rho endocytosed within large vesicles. Cellular location of lysosomes is mainly proximal to the nuclei, which explains the superposition of these cell compartments on merged microphotographs. Colocalization of USPIO-PHO-rho with lysosomes was infrequent, thus the microphotograph shown in Fig. 9B is

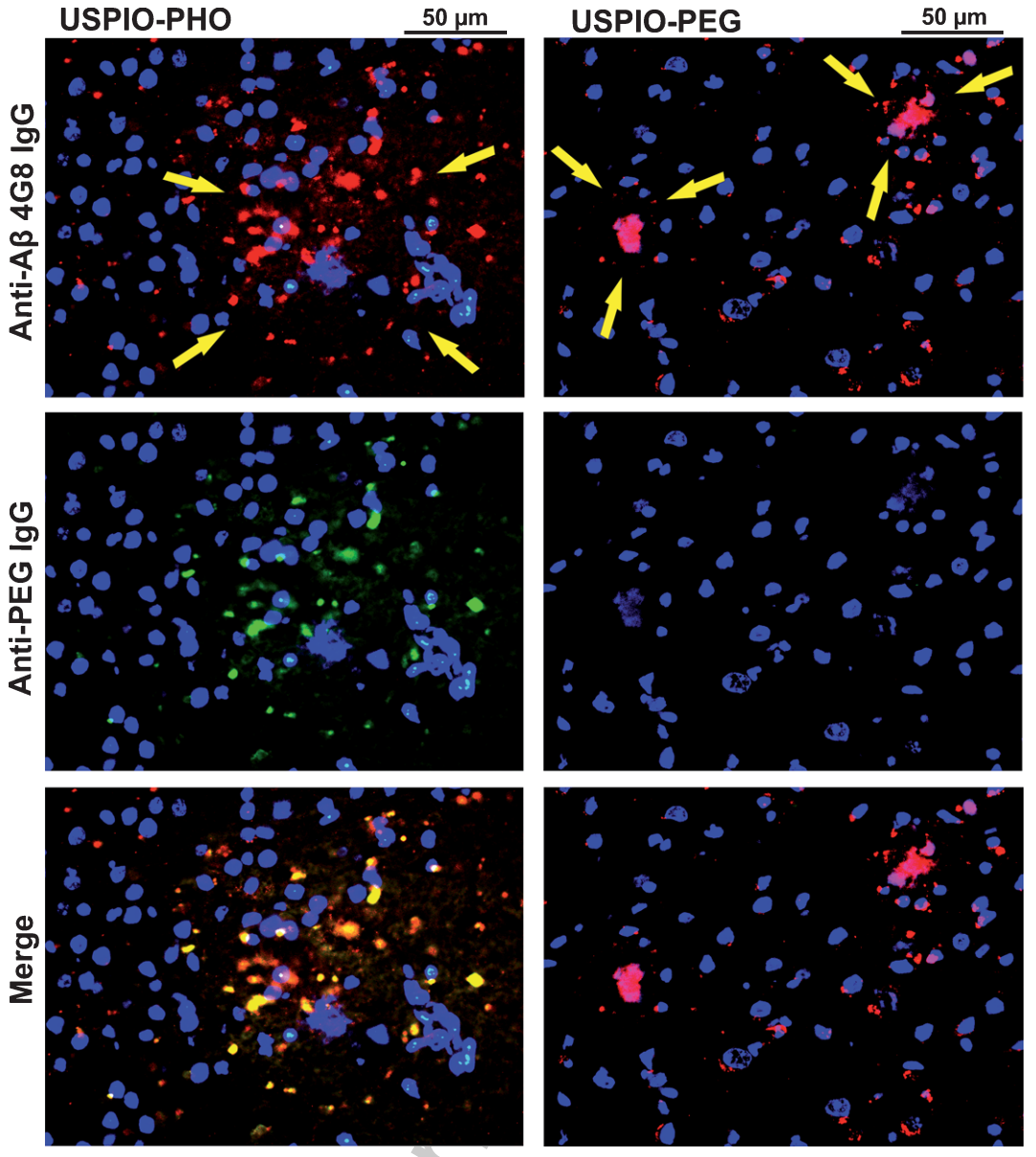

Fig. 8. Colocalization by immunofluorescence of AP and Aβ aggregates (anti-$A\beta_{17-24}$ 4G8 antibody, stained in red) with USPIO-PHO (anti-PEG antibody, stained in green) is compared to USPIO-PEG in the cortex of ADMM mice. The nuclei are stained in blue with DAPI. To note the pyknotic and fused nuclei within AP that are pointed with arrows. Some cells seem to contain Aβ in their cell bodies. The colocalization of USPIO-PHO with Aβ is revealed by the yellow/orange color of the merged microphotographs.

representative of this rare event. USPIO-PEG-rho could not be observed in either of the endocytic vesicles of this type of endothelial cells, which confirms its inability to cross the BBB. This CA was not observed either in the endothelial cells of the BBB in ADMM mice, but it seems to diffuse slightly through the blood–cerebrospinal fluid barrier (BCSFB) of the choroid plexus (data not shown), which is consistent with our previous observations [16]. Overall, these *in vitro* results corroborate our present and precedent studies with regard to the ability of USPIO-PHO to cross the endothelial cells of BBB via the non-degradation pathway associated with caveolae.

Conclusions

The development of diagnostic tools for AD is an essential step toward a better management of patients

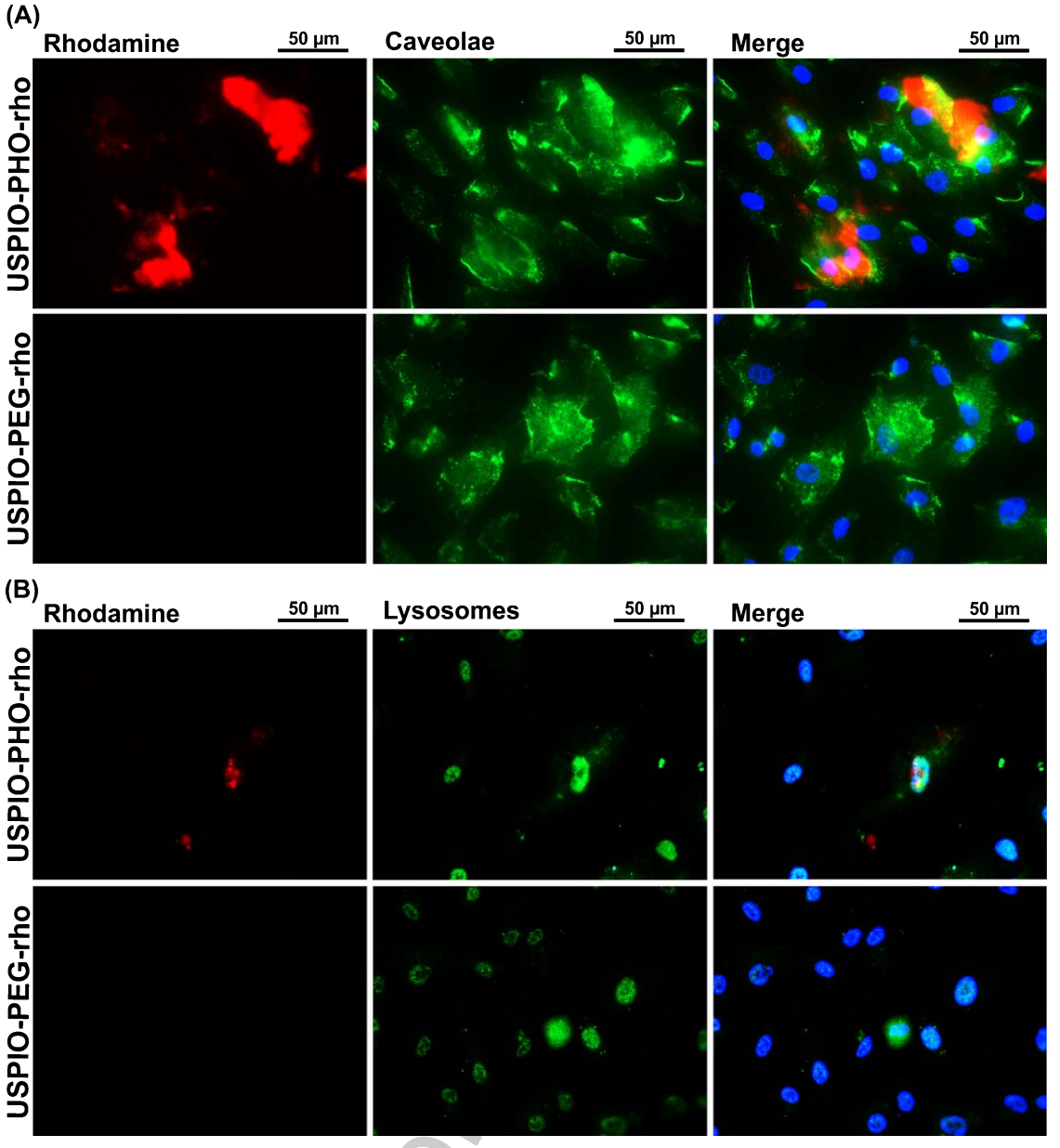

Fig. 9. Colocalization of USPIO-PHO-rho and USPIO-PEG-rho with caveolae (A) and lysosomes (B) in ACBRI376 human brain microvascular endothelial cells. USPIO derivatives are stained in red due to the coupled rhodamine, caveolae and lysosomes are stained in green with fluorescein, while nuclei are stained in blue with DAPI.

from the very first stages of the cognitive decline. Nowadays, definitive diagnosis of this pathology is performed postmortem by the histopathologic analysis of the brains. Nevertheless, the clinical diagnosis based on physical and neurological examinations of the patient, the detection of biomarkers using laboratory tests and neuroimaging obtains an accuracy higher than 90% [3]. Although useful, biomarkers' detection remains, however, controversial. For instance, $A\beta_{42}$ detection in the cerebrospinal fluid (CSF) does not include oligomers, leading to a bias in results' interpretation, and is limited by low concentrations [32]. Moreover, CSF sample collection is invasive and its routine implementation is challenging. Among the blood plasma biomarkers (T-tau, P-tau, and $A\beta_{42}$), P-tau seems to be the only one that discriminates AD patients from healthy controls, but its validity needs to be certified on larger cohorts [33].

Unfortunately, the molecular mechanisms of neurodegeneration precede by more than 20 years the clinical signs of AD, rendering fastidious the development of optimal therapeutic strategies [3].

Neuroimaging is a promising approach for the non-invasive diagnosis of AD, where Aβ deposits are the principal molecular imaging biomarker. Although PET tracers were the first compounds approved by the FDA and are still useful for AD diagnosis [34], MRI shows interesting benefits such as a better spatial resolution and the use of more specific and non-nuclear agents.

In the context of the above-mentioned shortcomings of the AD diagnosis, we propose a new MRI CA composed of USPIO functionalized with a cyclic heptapeptide (USPIO-PHO) specific to Aβ for the early diagnosis of AD. Considering its ability to recognize this molecular biomarker independently of its state of aggregation, USPIO-PHO may have an advantage over the nuclear tracers proposed so far. These imaging probes are specific to beta sheet-enriched structures like those in amyloid protein aggregates, which could explain their failure to discriminate amyloid burden associated with demented or non-demented elderly subjects. Moreover, USPIO are a class of superparamagnetic CAs showing important characteristics for molecular neuroimaging, such as an excellent nuclear magnetic resonance efficacy, low toxicity, relatively short half-life to allow for iterative acquisitions and the capacity to cross the BBB [35].

Contrary to most of the Aβ-targeted MRI tracers developed until now [12–14, 36], the specificity of our vectorized nanoparticles is not ensured by the Aβ peptide itself or by an anti-Aβ antibody, but is provided by the PHO peptide (C-IPLPFYN-C) identified by phage display [15]. The characterization of USPIO-PHO was previously performed and showed optimal features in terms of affinity, toxicity, biodistribution, pharmacokinetics, and BBB crossing [16].

In the present work, the usefulness of USPIO-PHO as a diagnosis tool has been evaluated on transgenic mouse models of AD (TG2576 and APP/PS1 dE9). MRI experiments revealed the significant accumulation of USPIO-PHO in the brains of ADMM mice, which was not equivalent to that of control CA USPIO-PEG or to the transgenic mice free of Aβ or AP. The darkening produced by USPIO-PHO on MR images of the brain was confirmed by the contrast analysis and the measurement of black pixels in post-contrast images, for all the ROI considered (cortex, hippocampus, thalamus, and the entire brain). These MRI data suggest, on the one hand, that USPIO-PHO can cross over the BBB, and on the other hand, that it could specifically detect Aβ aggregates in the AD brain. When co-injected with Cereport (a vasoactive mediator able to modulate tight junctions and open transiently the BBB) [25, 26], USPIO-PHO can accede inside the brain in a much larger quantity, but the quality of the contrasted molecular targets decreases due to the global negative contrast. In addition, Cereport enhances the clearance of USPIO-PHO from the targeted sites at 2-h post-injection, which is probably due to an amplified blood flow within the brain. However, this bradykinin analogue may contribute to the decrease of the injected dose of CA and to the visualization of cerebral molecular targets at shorter times after injection.

After brain collection, the presence of Aβ aggregates in the brains of ADMM mice was confirmed by immunohistochemistry. Aβ deposits were observed in cell bodies or between and over several cells that were included in the amyloid aggregates, contributing thus to the validation of molecular targets of USPIO-PHO. Perls'-DAB staining of USPIO-PHO in the brains of ADMM mice was consistent with the cell and tissue distribution of Aβ deposits detected by immunohistochemistry. Moreover, the high correlation coefficients found between the number of AP detected by Perls'-DAB staining or by immunohistochemistry plead for the specific targeting of this AD molecular hallmark by USPIO-PHO. The presence of USPIO-PHO, but not of USPIO-PEG, in endothelial cells of brain capillaries contributes to its validation as a BBB crossing agent. Consequently, the black pixels observed by MRI in the brain of ADMM mice injected with USPIO-PHO are likely reflecting the binding of this CA to its molecular target and thus the amyloid burden in AD. This assumption is furthermore sustained by the colocalization of USPIO-PHO with AP and Aβ deposits as observed by immunofluorescence. Altogether, these experimental data suggest that USPIO-PHO conserved its integrity after crossing over the BBB, being able to recognize Aβ peptide aggregated within the brain.

USPIO-PEG was found in the brain of ADMM mice, but its binding to AP was weaker, infrequent and mainly located at the border of AP. The presence of non-vectorized USPIO-PEG in the cerebral parenchyma is not surprising because of the PEG's ability to facilitate the brain access [37–39]. However, as previously observed by our group [16] and confirmed in the present work, USPIO-PEG seems to attain the brain via the BCSFB, where it was found in the choroid plexus.

Finally, the endocytosis of USPIO-PHO in endothelial cells of BBB seems to be mostly mediated by a non-degradation pathway through the caveolae, even if a small part of it is taken-up by lysosomes. USPIO-PEG does not seem to be endocytosed by this kind of cells, confirming the histochemistry studies and sustaining the hypothesis that its access into the brain does not occur via the BBB, but rather via the BCSFB. Present at the level of the choroid plexus, this barrier is less restrictive than the BBB because of weaker tight junctions [40, 41] associated with claudin-2 expression as opposed to BBB, which comprises claudin-4 known to decrease its permeability [42].

Although our USPIO derivatives may additionally penetrate the brain through a potentially leakier BBB of the aged AD mice [43, 44], this pathway does not seem to be the major mechanism borrowed by USPIO-PHO that is able to cross even the intact BBB of healthy NMRI mice [16]. Besides, a more permeable BBB should induce a similar penetration of USPIO-PHO and USPIO-PEG in AD mice brains. The higher negative contrast produced by USPIO-PHO, corroborated by histochemistry and immunohistochemistry studies, proves that this is not the case.

To conclude, the results presented in the present work support the idea that USPIO-PHO is able to cross the BBB and target AP, bringing the proof of concept that AD diagnosis could be performed non-invasively by MRI, potentially even at early stages of the disease, with peptide-functionalized imaging probes targeted to Aβ independently of its state of aggregation.

ACKNOWLEDGMENTS

This work is supported by the SAO-FRMA (Stichting voor Alzheimer Onderzoek – Fondation pour la Recherche sur la Maladie d'Alzheimer) foundation for Alzheimer's Research (grant number 11023), by the UMons-100 fellowship, and the FNRS (Fond National de la Recherche Scientifique). The ARC (Actions de Recherche Concertée) programs of the French Community of Belgium, Interreg program, the Walloon Region (Holocancer, Gadolymph programs) and COST actions are also gratefully acknowledged. The authors thank the Center for Microscopy and Molecular Imaging (CMMI, supported by the European Regional Development Fund and the Federation Wallonia Brussels). Guerbet Company is gratefully acknowledged for providing the transgenic mice TG2576 and APP/PS1 dE9.

Authors' disclosures available online (http://j-alz.com/manuscript-disclosures/17-0563r1).

SUPPLEMENTARY MATERIAL

The supplementary material is available in the electronic version of this article: http://dx.doi.org/10.3233/JAD-170563.

REFERENCES

[1] Burke JF, Langa KM, Hayward RA, Albin RL (2014) Modeling test and treatment strategies for presymptomatic Alzheimer disease. *PLoS One* **9**, e114339.

[2] World Alzheimer Report 2015, http://www.worldalzreport2015.org/downloads/world-alzheimer-report-2015.pdf, Last updated August 2015, Accessed on June 15, 2017.

[3] Chintamaneni M, Bhaskar M (2012) Biomarkers in Alzheimer's disease: A review. *ISRN Pharmacol* **2012**, 984786.

[4] Barage SH, Sonawane KD (2015) Amyloid cascade hypothesis: Pathogenesis and therapeutic strategies in Alzheimer's disease. *Neuropeptides* **52**, 1-18.

[5] Hardy J, Selkoe DJ (2002) The amyloid hypothesis of Alzheimer's disease: Progress and problems on the road to therapeutics. *Science* **297**, 353-356.

[6] Potter R, Patterson BW, Elbert DL, Ovod V, Kasten T, Sigurdson W, Mawuenyega K, Blazey T, Goate A, Chott R, Yarasheski KE, Holtzman DM, Morris JC, Benzinger TLS, Bateman RJ (2013) Increased in vivo amyloid-β42 production, exchange, and loss in presenilin mutation carriers. *Sci Transl Med* **5**, 189ra77.

[7] Reitz C (2012) Alzheimer's disease and the amyloid cascade hypothesis: A critical review. *Int J Alzheimers Dis* **2012**, 369808.

[8] Sorrentino P, Iuliano A, Polverino A, Jacini F, Sorrentino G (2014) The dark sides of amyloid in Alzheimer's disease pathogenesis. *FEBS Lett* **588**, 641-652.

[9] Zubenko GS (1997) Molecular neurobiology of Alzheimer's disease (syndrome?). *Harv Rev Psychiatry* **5**, 177-213.

[10] Villemagne VL (2016) Amyloid imaging: Past, present and future perspectives. *Ageing Res Rev* **30**, 95-106.

[11] Tong H, Lou K, Wang W (2015) Near-infrared fluorescent probes for imaging of amyloid plaques in Alzheimer's disease. *Acta Pharm Sin B* **5**, 25-33.

[12] Wadghiri YZ, Li J, Wang J, Hoang DM, Sun Y, Xu H, Tsui W, Li Y, Boutajangout A, Wang A, de Leon M, Wisniewski T (2013) Detection of amyloid plaques targeted by bifunctional USPIO in Alzheimer's disease transgenic mice using magnetic resonance microimaging. *PLoS One* **8**, e57097.

[13] Plissonneau M, Pansieri J, Heinrich-Balard L, Morfin JF, Stransky-Heilkron N, Rivory P, Mowat P, Dumoulin M, Cohen R, Allémann É, Tóth É, Saraiva MJ, Louis C, Tillement O, Forge V, Lux F, Marquette C (2016) Gd-nanoparticles functionalization with specific peptides for ß-amyloid plaques targeting. *J Nanobiotechnology* **14**, 60.

[14] Yin Z, Yul T, Xu Y (2015) Preparation of amyloid immuno-nanoparticles as potential mri contrast agents for Alzheimer's disease diagnosis. *J Nanosci Nanotechnol* **15**, 6429-6434.

[15] Larbanoix L, Burtea C, Laurent S, Van Leuven F, Toubeau G, Vander Elst L, Muller RN (2010) Potential amyloid plaque-specific peptides for the diagnosis of Alzheimer's disease. *Neurobiol Aging* **31**, 1679-1689.

[16] Ansciaux E, Burtea C, Laurent S, Crombez D, Nonclercq D, Vander Elst L, Muller RN (2015) In vitro and *in vivo* characterization of several functionalized ultrasmall particles of iron oxide, vectorized against amyloid plaques and potentially able to cross the blood-brain barrier: Toward earlier diagnosis of Alzheimer's disease by molecular imaging. *Contrast Media Mol Imaging* **10**, 211-224.

[17] Burtea C, Ballet S, Laurent S, Rousseaux O, Dencausse A, Gonzalez W, Port M, Corot C, Vander Elst L, Muller RN (2012) Development of a magnetic resonance imaging protocol for the characterization of atherosclerotic plaque by using vascular cell adhesion molecule-1 and apoptosis-targeted ultrasmall superparamagnetic iron oxide derivatives. *Arterioscler Thromb Vasc Biol* **32**, e36-48.

[18] Burtea C, Laurent S, Crombez D, Delcambre S, Sermeus C, Millard I, Rorive S, Flamez D, Beckers MC, Salmon I, Vander Elst L, Eizirik DL, Muller RN (2015) Development of a peptide-functionalized imaging nanoprobe for the targeting of (FXYD2)γa as a highly specific biomarker of pancreatic beta cells. *Contrast Media Mol Imaging* **10**, 398-412.

[19] Burtea C, Laurent S, Sanli T, Fanfone D, Devalckeneer A, Sauvage S, Beckers MC, Rorive S, Salmon I, Vander Elst L, Lauwerys BR, Muller RN (2016) Screening for peptides targeted to IL-7Rα for molecular imaging of rheumatoid arthritis synovium. *Arthritis Res Ther* **18**, 230.

[20] Larbanoix L, Burtea C, Ansciaux E, Laurent S, Mahieu I, Vander Elst L, Muller RN (2011) Design and evaluation of a 6-mer amyloid-beta protein derived phage display library for molecular targeting of amyloid plaques in Alzheimer's disease: Comparison with two cyclic heptapeptides derived from a randomized phage display library. *Peptides* **32**, 1232-1243.

[21] Stanicki D, Boutry S, Laurent S, Wacheul L, Nicolas E, Crombez D, Elst LV, Lafontaine DLJ, Muller RN (2013) Carboxy-silane coated iron oxide nanoparticles: A convenient platform for cellular and small animal imaging. *J Mater Chem B* **2**, 387-397.

[22] Hsiao K, Chapman P, Nilsen S, Eckman C, Harigaya Y, Younkin S, Yang F, Cole G (1996) Correlative memory deficits, Abeta elevation, and amyloid plaques in transgenic mice. *Science* **274**, 99-102.

[23] Savonenko A, Xu GM, Melnikova T, Morton JL, Gonzales V, Wong MP, Price DL, Tang F, Markowska AL, Borchelt DR (2005) Episodic-like memory deficits in the APPswe/PS1dE9 mouse model of Alzheimer's disease: Relationships to beta-amyloid deposition and neurotransmitter abnormalities. *Neurobiol Dis* **18**, 602-617.

[24] Oddo S, Caccamo A, Shepherd JD, Murphy MP, Golde TE, Kayed R, Metherate R, Mattson MP, Akbari Y, LaFerla FM (2003) Triple-transgenic model of Alzheimer's disease with plaques and tangles: Intracellular Abeta and synaptic dysfunction. *Neuron* **39**, 409-421.

[25] Bartus RT, Snodgrass P, Marsh J, Agostino M, Perkins A, Emerich DF (2000) Intravenous cereport (RMP-7) modifies topographic uptake profile of carboplatin within rat glioma and brain surrounding tumor, elevates platinum levels, and enhances survival. *J Pharmacol Exp Ther* **293**, 903-911.

[26] Saaber D, Wollenhaupt S, Baumann K, Reichl S (2014) Recent progress in tight junction modulation for improving bioavailability. *Expert Opin Drug Discov* **9**, 367-381.

[27] Ghiso J, Fossati S, Rostagno A (2014) Amyloidosis associated with cerebral amyloid angiopathy: Cell signaling pathways elicited in cerebral endothelial cells. *J Alzheimers Dis* **42**(Suppl 3):S167-76.

[28] Friedrich RP, Tepper K, Rönicke R, Soom M, Westermann M, Reymann K, Kaether C, Fändrich M (2010) Mechanism of amyloid plaque formation suggests an intracellular basis of Abeta pathogenicity. *Proc Natl Acad Sci USA* **107**, 1942-1947.

[29] Pagani L, Eckert A (2011) Amyloid-Beta interaction with mitochondria. *Int J Alzheimers Dis* 2011, 925050.

[30] Revett TJ, Baker GB, Jhamandas J, Kar S (2013) Glutamate system, amyloid ß peptides and tau protein: Functional interrelationships and relevance to Alzheimer disease pathology. *J Psychiatry Neurosci* **38**, 6-23.

[31] Bayer TA, Wirths O (2010) Intracellular accumulation of amyloid-Beta - a predictor for synaptic dysfunction and neuron loss in Alzheimer's disease. *Front Aging Neurosci* **2**, 8.

[32] Humpel C, Hochstrasser T (2011) Cerebrospinal fluid and blood biomarkers in Alzheimer's disease. *World J Psychiatry* **1**, 8-18.

[33] Olsson B, Lautner R, Andreasson U, Öhrfelt A, Portelius E, Bjerke M, Hölttä M, Rosén C, Olsson C, Strobel G, Wu E, Dakin K, Petzold M, Blennow K, Zetterberg H (2016) CSF and blood biomarkers for the diagnosis of Alzheimer's disease: A systematic review and meta-analysis. *Lancet Neurol* **15**, 673-684.

[34] Torosyan N, Silverman DHS (2014) New PET tracers for dementia evaluation: Coming to your clinic now. *Appl Radiol* 2014435.

[35] Winer JL, Kim PE, Law M, Liu CY, Apuzzo ML (2011) Visualizing the future: Enhancing neuroimaging with nanotechnology. *World Neurosurg* **75**, 626-637; discussion 618-619.

[36] Ramakrishnan M, Wengenack TM, Kandimalla KK, Curran GL, Gilles EJ, Ramirez-Alvarado M, Lin J, Garwood M, Jack CR, Poduslo JF (2008) Selective contrast enhancement of individual Alzheimer's disease amyloid plaques using a polyamine and Gd-DOTA conjugated antibody fragment against fibrillar Abeta42 for magnetic resonance molecular imaging. *Pharm Res* **25**, 1861-1872.

[37] Calvo P, Gouritin B, Villarroya H, Eclancher F, Giannavola C, Klein C, Andreux JP, Couvreur P (2002) Quantification and localization of PEGylated polycyanoacrylate nanoparticles in brain and spinal cord during experimental allergic encephalomyelitis in the rat. *Eur J Neurosci* **15**, 1317-1326.

[38] Kolate A, Baradia D, Patil S, Vhora I, Kore G, Misra A (2014) PEG - a versatile conjugating ligand for drugs and drug delivery systems. *J Control Release* **192**, 67-81.

[39] Nance EA, Woodworth GF, Sailor KA, Shih TY, Xu Q, Swaminathan G, Xiang D, Eberhart C, Hanes J (2012) A dense poly(ethylene glycol) coating improves penetration of large polymeric nanoparticles within brain tissue. *Sci Transl Med* **4**, 149ra119.

[40] Neuwelt EA, Bauer B, Fahlke C, Fricker G, Iadecola C, Janigro D, Leybaert L, Molnár Z, O'Donnell ME, Povlishock JT, Saunders NR, Sharp F, Stanimirovic D, Watts RJ, Drewes LR (2011) Engaging neuroscience to advance translational research in brain barrier biology. *Nat Rev Neurosci* **12**, 169-182.

[41] Strazielle N, Ghersi-Egea JF (2013) Physiology of blood-brain interfaces in relation to brain disposition of small compounds and macromolecules. *Mol Pharm* **10**, 1473-1491.

[42] Van Itallie CM, Holmes J, Bridges A, Gookin JL, Coccaro MR, Proctor W, Colegio OR, Anderson JM (2008) The density of small tight junction pores varies among cell types and is increased by expression of claudin-2. *J Cell Sci* **121**, 298-305.

[43] Biron KE, Dickstein DL, Gopaul R, Jefferies WA (2011) Amyloid triggers extensive cerebral angiogenesis causing blood brain barrier permeability and hypervascularity in Alzheimer's disease. *PLoS One* **6**, e23789.

[44] Minogue AM, Jones RS, Kelly RJ, McDonald CL, Connor TJ, Lynch MA (2014) Age-associated dysregulation of microglial activation is coupled with enhanced blood-brain barrier permeability and pathology in APP/PS1 mice. *Neurobiol Aging* **35**, 1442-1452.